Computational Mechanics manuscript No.
(will be inserted by the editor)

Computational modeling of hypertensive growth in the human carotid artery

P. Sáez[1,2], E. Peña[1,2], M.A. Martínez[1,2], Ellen Kuhl[3]

[1] Group of Applied Mechanics and Bioengineering, Aragón Institute of Engineering Research, University of Zaragoza, Spain.
[2] CIBER-BBN. Centro de Investigación Biomédica en Red en Bioingeniería, Biomateriales y Nanomedicina, Spain.
[3] Departments of Mechanical Engineering, Bioengineering, and Cardiothoracic Surgery, Stanford University, CA 94305, USA.

Received: 12.08.13 / Revised version: XX.XX.XX

Abstract Arterial hypertension is a chronic medical condition associated with an elevated blood pressure. Chronic arterial hypertension initiates a series of events, which are known to collectively initiate arterial wall thickening. However, the correlation between macrostructural mechanical loading, microstructural cellular changes, and macrostructural adaptation remains unclear. Here, we present a microstructurally motivated computational model for chronic arterial hypertension through smooth muscle cell growth. To model growth, we adopt a classical concept based on the multiplicative decomposition of the deformation gradient into an elastic part and a growth part. Motivated by clinical observations, we assume that the driving force for growth is the stretch sensed by the smooth muscle cells. We embed our model into a finite element framework, where growth is stored locally as an internal variable. First, To demonstrate the features of our model, we investigate the effects of hypertensive growth in a real human carotid artery. Our results agree nicely with experimental data reported in the literature both qualitatively and quantitatively.

Key words Biomechanics; growth; smooth muscle cells; hypertension; finite element method

1 Motivation

Hypertension is characterized through a substantial elevation in blood pressure, which initiates the adaptation of vascular tissue. The immediate change, on a short-term scale, is the adaptation of smooth muscle cell (SMC) contractile forces in the connective tissue, which can reduce the lumen diameter to compensate for the extra stresses. In addition, we can observe two long-term adaptation processes. The first long-term change is related to the secretion of collagen in the extracellular matrix, which gradually stiffens the arterial tissue.

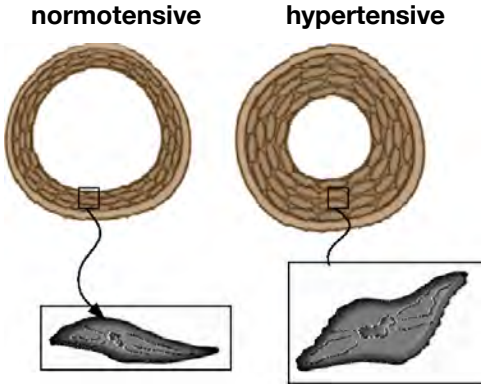

Fig. 1 Hypertensive anisotropic arterial growth. In contrast to the normtensive artery (left), the hypertensive artery (right) displays progressive smooth muscle cell growth resulting in chronic arterial wall thickening.

The second long-term change consists of the increase of SMCs both in volume and in number. Experimentally, this adaptation manifests itself in a thickening of the vessel wall. In this work, we focus on this latter phenomenon, the growth of SMC in response to chronic hypertension.

SMCs are responsible for vascular contraction, also known as myogenic tone [6, 56], which is directly related to the intracellular calcium concentration and to the ion channels of the cell [7]. This force attempts to compensate the over-stress in the vessel wall to maintain the same vessel diameter [23, 46].

SMCs typically grow through hypertrophy, by increasing their volume, through hyperplasia, by increasing their number, or through a combination of both [47, 49]. This micro-structural change leads to the well-documented thickening of the vessel wall to restore the homeostatic stress state illustrated in Figure 1. These changes are more pronounced in small or resistance vessels [12, 44]. A multitude of experimental findings is related to hypertension-induced thickening of the arterial

wall; many of them are related to drug performance, to the genetic expression of substances, and to the plain case of thickening. Some of these studies look at essential hypertension while other asses hypertension by means of hypoxic states or ligands of some particular arteries.

Wiener et al. [62] studied aorta arteries of rats and observed a decrease of the lumen diameter of 9% while the thickness increased by 18% from 182.5μm in the normotensive state to 215.5μm in hypertension. Owens and Schwartz [49] reported an increase of 35% in SMC size due to hyperplasia also in aorta of rat. The same authors showed an increase of 39.67% and a 21.16% in SMC mass in a different type of rats [48]. Schofield et al. [55] looked at the evolution of small human arteries and observed that internal diameter decreased from 140μm to 118μm, while thickness increased by 46.39%. Since smaller arteries display a more pronounced contractile response, such a drastic decrease could be caused by contractile phenomena. In fact, the above studies also addressed changes in the miogenic response in response to hypertension.

Studies on the carotid artery are also numerous. Boutouyrie et al. [5] reported a rise of the internal diameter in human carotids from 5.25 mm to 5.66 mm and an increase in thickness of 27.27% from 0.487 mm to 0.572 mm. However, the same work showed a slight decrease in the lumen diameter from 2.33 mm to 2.32 mm in the radial artery accompanied by a 21.98% increase in thickness. Fridez et al. [13] studied the influence of hypertension in carotid arteries of rats. They showed that the internal radius increased in hypertensive rats but it increased at slower rate than in the control group. The thickness increased by 58.4% from 142 μm to 225 μm. However, this represented just a 30% increase with respect to control group. The same group also observed that the thickness of outer lamelar units grew more than those of inner units. Eberth et al. [8] also studied the morphological changes in the carotids of rats and reported an increase in the internal radius from 531 μm to 592 μm while the thickness increases from 23.1 μm to 85.7 μm after 56 weeks.

These results demonstrate how vascular adaptation can differ, not only between different arteries and species but also with the same artery of the same species. Variation from specimen to specimen, different degrees of SMC activation, genetic disorders, age, life style, and many more factors can be a cause of this variability. To point out a last example, Feihl et al. [10] collected data from different authors who all studied small subcutaneous human arteries. While there was a strong quantitative variability in the adaptive response, the qualitative trends were all similar to the trends described above.

The computational study of growth has gained increasing attention in the theoretical and computational mechanics community, [1, 28, 43, 59]. Mechanical modeling of growth has been addressed in different ways. Typically, growing biological tissues are considered as open systems [35]. Their different configurational settings and their numerical treatment within the finite element method are discussed in Kuhl and Steinmann [34]. Typically, we can distinguish two fundamental forms of growth: volume growth [24] and density growth [33]. The first allows for changes in volume while keeping the density constant while the second maintains a constant volume while the density is allowed to change [36, 41, 42]. The works of Skalak et al. [57] and Rodriguez et al. [51] pioneered the underlying kinematic description of volumetric growth. Within the past decade, various authors and groups have adopted and refined this concept [15,22,30]. An alternative approach towards growth is based on the constrained mixture theory, where several constituents of a tissue are allowed to growth independently [27,29]. A similar approach [18,19,32] was recently extended to reactive mixtures [2]. We would also like to point out the early work of Fung and Liu [14], which demonstrates that the growth of blood vessels induces a change in the natural configuration, associated with the notion of residual stress.

The goal of this work is to present a computational model of volumetric growth for SMC based on the anisotropic microstructure of the vascular tissue. We adapt a well-established growth model and its underlying consistent numerical procedure. We focus on SMC growth in response to chronic hypertension and on its impact on arterial wall thickening. First, we briefly reiterate the general mechanical background of soft tissue and growth mechanics used in this work. Then, based on experimental data, we will compute a simple case of hypertension that allows us to calibrate the material parameters of our model. In particular, we model growth of SMC as a stretch-driven process, activated by an elevated pressure. We update the state of growth implicitly by means of a Newton-Raphson scheme. Finally, we present a real human carotid geometry to illustrate the features of our model, before we close by discussing the main conclusions of our work.

2 Baseline elasticity of cardiovascular tissue

Two important aspects enter the mechanical description of the cardiovascular tissue, the kinematically non-linear behavior of quasi-incompressible materials and constitutively non-linear behavior of quasi-incompressible materials. We will briefly summarize both in the following subsections.

2.1 Kinematics of quasi-incompressiblity

First, we reiterate the basic equations of the kinematically non-linear behavior. Our key kinematic quantity is the deformation gradient, the tangent of the motion,

represented by a two-point linear mapping over the reference configuration. Based on the motion $\boldsymbol{\varphi}$, we define the deformation gradient as

$$\mathbf{F} = \nabla_{\mathbf{X}} \boldsymbol{\varphi} \tag{1}$$

and denote its Jacobians as $\mathrm{J} = \det(\mathbf{F})$. We can then introduce the right Cauchy Green tensor

$$\mathbf{C} = \mathbf{F}^{\mathrm{t}} \cdot \mathbf{F} \tag{2}$$

as a characteristic deformation measure. Moreover, we can introduce the spatial velocity gradient $\mathbf{l} = \dot{\mathbf{F}} \cdot \mathbf{F}^{-1} = \nabla_x \mathbf{v}$ in terms of the velocity $\mathbf{v} = \dot{\boldsymbol{\varphi}}$, where $\{\dot{\circ}\} = \partial_{\mathrm{t}} \{\circ\} |_{\mathbf{X}}$ denotes the time derivative at fixed material position $\mathbf{X}$. The symmetric part of the spatial velocity gradient defines the spatial rate of deformation tensor $\mathbf{d} = \mathbf{l}^{\mathrm{sym}}$. To account for the characteristic quasi-incompressibile behavior of soft biological tissues, we adopt a volumetric-isochoric decomposition of the deformation gradient [11, 16],

$$\mathbf{F} = \mathrm{J}^{1/3} \bar{\mathbf{F}} \,. \tag{3}$$

The overbar is associated with the prefix isochoric and denotes the volume-preserving part. Accordingly, $\bar{\mathbf{F}}$ denotes the isochoric deformation gradient with $\det(\bar{\mathbf{F}}) = 1$, and

$$\bar{\mathbf{C}} = \bar{\mathbf{F}}^{\mathrm{t}} \cdot \bar{\mathbf{F}} \tag{4}$$

denotes the associated isochoric right Cauchy Green tensor. It proves convenient to introduce its first and fourth invariants,

$$\bar{I}_1 = \bar{\mathbf{C}} : \mathbf{I} \qquad \text{and} \qquad \bar{I}_4 = \bar{\mathbf{C}} : \mathbf{N} \tag{5}$$

where $\mathbf{N} = \boldsymbol{n} \otimes \boldsymbol{n}$ denotes the structural tensor defined in terms of the characteristic microstructural direction $\boldsymbol{n}$.

2.2 Constitutive equations of quasi-incompressibility

Second, we summarize the basic equations of the constitutively non-linear behavior. For soft biological tissues it is common to adapt the framework of hyperlasticity, based on the definition of a strain energy density function Ψ. To account for the quasi-incompressible behavior, we additively decompose this strain energy density function into a volumetric and isochoric parts,

$$\Psi = \Psi_{\mathrm{vol}}(\mathrm{J}) + \Psi_{\mathrm{iso}}(\bar{\mathbf{C}}) \,. \tag{6}$$

The first term, the volumetric contribution Ψ_{vol}, is primarily related to the water content in the tissue. The second term, the isochoric contribution Ψ_{iso}, is typically further split into an isotropic contribution related to the elastin content Ψ_{ela} and an anisotropic contribution related to the collagen fibers Ψ_{col}. From the evaluation of the dissipation inequality [25, 40], we obtain the second Piola-Kirchhoff stress tensor,

$$\mathbf{S} = 2\partial_{\mathbf{C}} \Psi = \mathbf{S}_{\mathrm{vol}} + \mathbf{S}_{\mathrm{iso}} \tag{7}$$

which consists of a volumetric part,

$$\mathbf{S}_{\mathrm{vol}} = 2\partial_{\mathbf{C}} \Psi_{\mathrm{vol}} = \mathrm{J}\, \partial_{\mathrm{J}} \Psi_{\mathrm{vol}}\, \mathbf{C}^{-1} \,, \tag{8}$$

and an isotropic part,

$$\mathbf{S}_{\mathrm{iso}} = 2\partial_{\mathbf{C}} \Psi_{\mathrm{iso}} = 2\partial_{\bar{\mathbf{C}}} \Psi_{\mathrm{iso}} : \partial_{\mathbf{C}} \bar{\mathbf{C}} = \mathrm{J}^{-2/3} \mathbb{P} : \bar{\mathbf{S}} \,. \tag{9}$$

Here $\bar{\mathbf{S}} = \partial_{\bar{\mathbf{C}}} \Psi_{\mathrm{iso}}$ is the fictitious second Piola-Kirchhoff stress and $\mathbb{P}$ denotes the fourth order projection tensor defined as $\mathbb{P} = \mathbb{I} - \frac{1}{3}\, \mathbf{C}^{-1} \otimes \mathbf{C}$. By applying the contravariant push forward operation, we obtain the Cauchy stress $\boldsymbol{\sigma}$ for the finite element implementation,

$$\boldsymbol{\sigma} = \frac{1}{\mathrm{J}}\, \mathbf{F} \cdot \mathbf{S} \cdot \mathbf{F}^{\mathrm{t}} \,. \tag{10}$$

The tensor of tangent moduli, a fourth order tensor that relates stress and strain increments, is essential for a consistent finite element implementation. It represents the total derivative of the stress $\mathbf{S}$ with respect to the deformation tensor $\mathbf{C}$,

$$\mathbf{C} = 2\mathrm{d}_{\mathbf{C}} \mathbf{S} = \mathbf{C}_{\mathrm{vol}} + \mathbf{C}_{\mathrm{iso}} \,, \tag{11}$$

and consists of a volumetric contribution,

$$\mathbf{C}_{\mathrm{vol}} = 2\mathrm{d}_{\mathbf{C}} \mathbf{S}_{\mathrm{vol}} = 2\,\mathrm{J}\, \tilde{p}\, \mathbf{C}^{-1} \otimes \mathbf{C}^{-1} - 2\,\mathrm{J}\, p\, \mathbb{I}_{\mathrm{C}^{-1}} \,, \tag{12}$$

and an isochoric contribution,

$$\begin{aligned} \mathbf{C}_{\mathrm{iso}} = 2\mathrm{d}_{\mathbf{C}} \mathbf{S}_{\mathrm{iso}} = \mathbb{P} : \overline{\mathbf{C}} : \mathbb{P}^{\mathrm{t}} - \tfrac{2}{3} \mathrm{tr}(\mathrm{J}^{-2/3} \mathbf{S}_{\mathrm{iso}}) \tilde{\mathbb{P}} \\ - \tfrac{2}{3} [\overline{\mathbf{S}} \otimes \mathbf{C}^{-1} + \mathbf{C}^{-1} \otimes \overline{\mathbf{S}}] \,, \end{aligned} \tag{13}$$

where p denotes the hydrostatic pressure and $\tilde{p} = p + \mathrm{J}\, \partial_{\mathrm{J}} p$. In addition, we have introduced the following abbreviations for the fourth order tensors $\tilde{\mathbb{P}} = \mathbb{I}_{\mathrm{C}^{-1}} - \frac{1}{3}\, \mathbf{C}^{-1} \otimes \mathbf{C}^{-1}$ and $\mathbb{I}_{\mathrm{C}^{-1}} = \frac{1}{2} [\mathbf{C}^{-1} \overline{\otimes} \mathbf{C}^{-1} + \mathbf{C}^{-1} \underline{\otimes} \mathbf{C}^{-1}]$, where the non-standard fourth order tensor products take the following interpretation, $\{\bullet \overline{\otimes} \circ\}_{ijkl} = \{\bullet\}_{ik}\, \{\circ\}_{jl}$ and $\{\bullet \underline{\otimes} \circ\}_{ijkl} = \{\bullet\}_{il}\, \{\circ\}_{jk}$.

Remark 1 (Elasticity of arterial tissue) *The modeling of arterial tissue has been widely described in literature [26]. It is common to describe the isochoric response Ψ_{iso} by means of an isotropic contribution Ψ_{ela} and an anisotropic contribution Ψ_{col}, related to the elastin and the collagen content, respectively. This feature can be described as*

$$\Psi_{\mathrm{iso}}(\bar{I}_1, \bar{I}_4) = \Psi_{\mathrm{ela}}(\bar{I}_1) + \Psi_{\mathrm{col}}(\bar{I}_4) \,,$$

where $\bar{I}_1$ and $\bar{I}_4$ are the first and fourth invariant of the isochoric part of the deformation according to equation (5). The isotropic part related to the elastin content, Ψ_{ela}, is typically parameterized in terms of a single stress-like material parameter μ, e.g., as

$$\Psi_{\mathrm{ela}}(\bar{I}_1) = \mu\, [\, \bar{I}_1 - 3 \,] \,.$$

Table 1 Material parameters for media and adventitia of human common carotid artery (CCA) and of human internal carotid artery (ICA) [54, 58].

	μ [kPa]	k_1 [kPa]	k_2 [-]
CCA media	4.31	2.19	4.15
CCA adventitia	0.04	7.32	66.81
ICA media	11.01	2.14	20.72
ICA adventitia	0.04	15.97	51.01

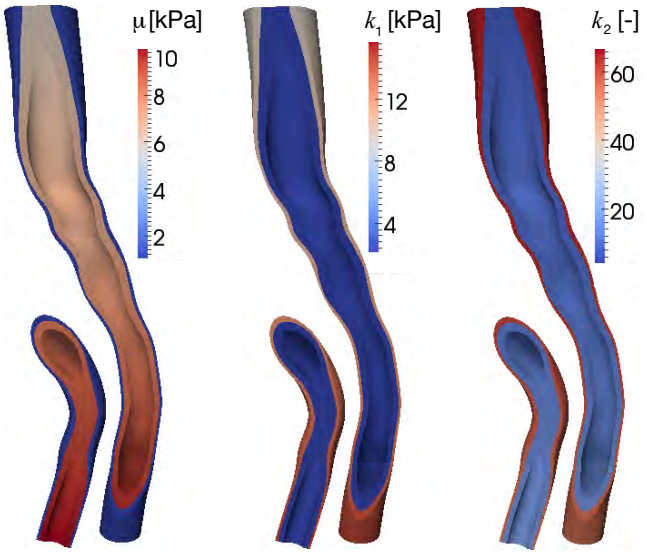

Fig. 2 Regional variation of material parameters μ, k_1, and k_2 along human carotid artery.

The anisotropic part related to the collagen content, Ψ_{col}, has been discussed intensely in the literature. O'Connell et al. [45] have studied the structural organization of the arterial layers, and found that the collagen fibers follow a helicoidal distribution from the outer to the inner layer. Collagen fibers are bundled around SMC and around some secondary fibrils, which cross-link the main collagen fibers. In the adventitia, the outermost layer of the artery, collagen displays a rather random distribution, while in the media layer, the middle layer, collagen and SMC forms several sublayers with slightly different preferential orientations. Garcia [17] reported an almost circumferential orientation of the collagen fibers in the media of carotid arteries. Here, for simplicity, we assume the following ansatz

$$\Psi_{\text{col}}(\bar{I}_1) = \frac{k_1}{2k_2}[\exp(k_2[\bar{I}_1 - 1]^2) - 1]\,.$$

Based on experimental data [58], we obtained the mechanical parameters in different regions of the human carotid artery. Table 1 summarizes the calibrated material parameter values. Figure 2 illustrates the regional variation of the mechanical parameters along the carotid artery.

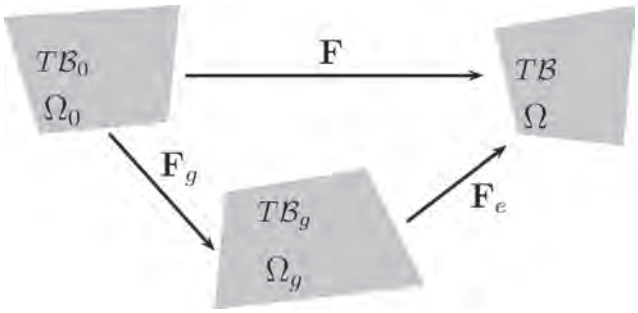

Fig. 3 Kinematic of growth. Composition of a elastic deformation gradient $\mathbf{F}_e$ and a growth tensor $\mathbf{F}_g$

3 Growth of cardiovascular tissue

3.1 Kinematics of growth

Within the framework of finite growth, the key kinematic assumption is the multiplicative decomposition of the deformation gradient $\mathbf{F}$ into an elastic part $\mathbf{F}_{\text{e}}$ and a growth part $\mathbf{F}_{\text{g}}$ [51],

$$\mathbf{F} = \mathbf{F}_{\text{e}} \cdot \mathbf{F}_{\text{g}}\,. \tag{14}$$

The underlying concept is adopted from the multiplicative decomposition in finite elastoplasticity [38]. While we can think of the growth tensor $\mathbf{F}_{\text{g}}$ as a second-order variable to characterize arbitrary forms of isotropic or anisotropic growth, here we will parameterize the growth tensor exclusively in terms of a single scalar-valued variable, the growth multiplier ϑ [20]. We denote the Jacobians of the elastic tensor and of the growth tensor as $\text{J}_{\text{e}} = \det(\mathbf{F}_{\text{e}})$ and $\text{J}_{\text{g}} = \det(\mathbf{F}_{\text{g}})$, respectively, such that $\text{J} = \text{J}_{\text{e}}\,\text{J}_{\text{g}}$. We can then introduce the elastic right Cauchy Green tensor $\mathbf{C}_{\text{e}}$ in the following form.

$$\mathbf{C}_{\text{e}} = \mathbf{F}_{\text{e}}^{\text{t}} \cdot \mathbf{F}_{\text{e}} = \mathbf{F}_{\text{g}}^{\text{-t}} \cdot \mathbf{C} \cdot \mathbf{F}_{\text{g}}^{\text{-1}} \tag{15}$$

The pull back of the spatial velocity gradient $\mathbf{l}$ to the intermediate configuration

$$\mathbf{F}_{\text{e}}^{\text{-1}} \cdot \mathbf{l} \cdot \mathbf{F}_{\text{e}} = \mathbf{L}_{\text{e}} + \mathbf{L}_{\text{g}} \tag{16}$$

introduces the additive decomposition into an elastic contribution $\mathbf{L}_{\text{e}}$ and a growth contribution $\mathbf{L}_{\text{g}}$,

$$\mathbf{L}_{\text{e}} = \mathbf{F}_{\text{e}}^{\text{-1}} \cdot \dot{\mathbf{F}}_{\text{e}} = \dot{\mathbf{F}}_{\text{e}} \cdot \mathbf{F}_{\text{e}}^{\text{-1}} \quad \text{and} \quad \mathbf{L}_{\text{g}} = \dot{\mathbf{F}}_{\text{g}} \cdot \mathbf{F}_{\text{g}}^{\text{-1}}, \tag{17}$$

such that the rate of deformation tensor of the intermediate configuration follows as $\mathbf{d}_{\text{g}} = \mathbf{l}_{\text{g}}^{\text{sym}}$ with $\mathbf{l}_{\text{g}} = \mathbf{F}_{\text{e}} \cdot \mathbf{L}_{\text{g}} \cdot \mathbf{F}_{\text{e}}^{\text{-1}}$. Figure 3 illustrates the kinematics of finite growth, the deformation tensors $\mathbf{C}$ and $\mathbf{C}_{\text{e}}$, and the mappings $\mathbf{F} = \mathbf{F}_{\text{e}} \cdot \mathbf{F}_{\text{g}}$ and $\mathbf{F}^{\text{-t}} = \mathbf{F}_{\text{e}}^{\text{-t}} \cdot \mathbf{F}_{\text{g}}^{\text{-t}}$ between tangent spaces and cotangent spaces.

Remark 2 (Growth of arterial tissue) *For the particular problem of growth in arterial tissue, we adopt the formulation proposed by Himpel et al. [24] and Göktepe*

et al. [21]. To account for experimental observations of SMC growth [47–49], we define the growth tensor as

$$\mathbf{F}_{\mathrm{g}} = \mathbf{I} + [\,\vartheta - 1\,]\,\mathbf{n}_{\mathrm{r}} \otimes \mathbf{n}_{\mathrm{r}}$$

where ϑ is the scalar-valued growth multiplier that defines the level of growth and $\mathbf{n}_{\mathrm{r}}$ characterizes the radial direction [50]. This particular format of the growth tensor characterizes smooth muscle cell thickening in the radial direction $\mathbf{n}_{\mathrm{r}}$ while the ellipsoidal muscle cells maintain the same length, see Figure **??***. Acutely, SMC maintain their original length by contracting. Chronically SMC grow in the radial direction to reduce elevated wall stresses Some experiments indicate that SMC may also contract in the axial direction, to decrease the lumen diameter. However, for simplicity, here we assume that the axial dimension remains constant.*

3.2 Constitutive equations of growth

Next, we embed the kinematic characterization of growth into the hyperelastic baseline description introduced in Section 2.2. To this end, we reparameterize the Helmholtz strain energy function $\Psi(\mathbf{C}_{\mathrm{e}})$, which was initially parameterized in terms of the elastic deformation tensor $\mathbf{C}_{\mathrm{e}}$, in terms of the total deformation tensor $\mathbf{C}$ and the growth tensor $\mathbf{F}_{\mathrm{g}}$, such that $\Psi(\mathbf{C}, \mathbf{F}_{\mathrm{g}})$ and

$$\dot{\Psi} = \partial_{\mathbf{C}}\Psi : \dot{\mathbf{C}} + \partial_{\mathbf{F}_{\mathrm{g}}}\Psi : \dot{\mathbf{F}}_{\mathrm{g}} \tag{18}$$

Thermodynamic considerations motivate the introduction of the second Piola-Kirchhoff stress,

$$\mathbf{S} = 2\partial_{\mathbf{C}}\Psi = 2\partial_{\mathbf{C}_{\mathrm{e}}}\Psi : \partial_{\mathbf{C}}\mathbf{C}_{\mathrm{e}} = \mathbf{F}_{\mathrm{g}}^{-1} \cdot \mathbf{S}_{\mathrm{e}} \cdot \mathbf{F}_{\mathrm{g}}^{-\mathrm{t}}\,, \tag{19}$$

with $\mathbf{S}_{\mathrm{e}} = \partial_{\mathbf{C}_{\mathrm{e}}}\Psi$. To derive the Lagrangian tangent moduli, essential for a consistent finite element implementation, we evaluate the total derivative of the $\mathbf{S}$ with respect to $\mathbf{C}$.

$$\begin{aligned}\mathbf{C} = 2\mathrm{d}_{\mathbf{C}}\mathbf{S} &= \mathbf{C}_{\mathrm{e}} + \mathbf{C}_{\mathrm{g}} \\ &= 2\partial_{\mathbf{C}}\mathbf{S}\big|_{\mathbf{F}_{\mathrm{g}}} + 2\partial_{\mathbf{C}}\mathbf{S}\big|_{\mathbf{F}} \\ &= 2\partial_{\mathbf{C}}\mathbf{S}\big|_{\mathbf{F}_{\mathrm{g}}} + 2\left[\partial_{\mathbf{F}_{\mathrm{g}}}\mathbf{S} : \partial_{\vartheta}\mathbf{F}_{\mathrm{g}}\right] \otimes \partial_{\mathbf{C}}\vartheta\big|_{\mathbf{F}}\end{aligned} \tag{20}$$

The first term of equation (20) represents the classical elastic tangent moduli, $2\mathrm{d}_{\mathbf{C}_{\mathrm{e}}}\mathbf{S}_{\mathrm{e}}$, pulled back to the undeformed reference configuration,

$$\mathbf{C}_{\mathrm{e}} = 2\mathrm{d}_{\mathbf{C}}\mathbf{S}\big|_{\mathbf{F}_{\mathrm{g}}} = [\mathbf{F}_{\mathrm{g}}^{-1}\overline{\otimes}\mathbf{F}_{\mathrm{g}}^{-1}] : 2\mathrm{d}_{\mathbf{C}_{\mathrm{e}}}\mathbf{S}_{\mathrm{e}} : [\mathbf{F}_{\mathrm{g}}^{-\mathrm{t}}\overline{\otimes}\mathbf{F}_{\mathrm{g}}^{-\mathrm{t}}]\,. \tag{21}$$

The second term of equation (20) is related to the linearization of the growth model,

$$\mathbf{C}_{\mathrm{g}} = 2\mathrm{d}_{\mathbf{C}}\mathbf{S}\big|_{\mathbf{F}} = 2\left[\partial_{\mathbf{F}_{\mathrm{g}}}\mathbf{S} : \partial_{\vartheta}\mathbf{F}_{\mathrm{g}}\right] \otimes \partial_{\mathbf{C}}\vartheta\big|_{\mathbf{F}} \tag{22}$$

where

$$\begin{aligned}\partial_{\mathbf{F}_{\mathrm{g}}}\mathbf{S} = &-[\,\mathbf{F}_{\mathrm{g}}^{-1}\overline{\otimes}\mathbf{S} + \mathbf{S}\underline{\otimes}\mathbf{F}_{\mathrm{g}}^{-1}\,] \\ &-[\,\mathbf{F}_{\mathrm{g}}^{-1}\overline{\otimes}\mathbf{F}_{\mathrm{g}}^{-1}\,] : \tfrac{1}{2}\,\mathbf{C} : [\,\mathbf{F}_{\mathrm{g}}^{-\mathrm{t}}\overline{\otimes}\mathbf{C}_{\mathrm{e}} + \mathbf{C}_{\mathrm{e}}\underline{\otimes}\mathbf{F}_{\mathrm{g}}^{-\mathrm{t}}]\,,\end{aligned} \tag{23}$$

while $\partial_{\vartheta}\mathbf{F}_{\mathrm{g}}$ and $\partial_{\mathbf{F}}\vartheta$ are specific of the chosen growth tensor $\mathbf{F}_{\mathrm{g}}$ and will be provided in following sections. To obtain the Eulerian tangent moduli $\mathbf{c}$ for the finite element implementation, we push Lagrangian tangent moduli $\mathbf{C}$ of equation (20) forward to the deformed configuration,

$$\mathbf{c} = \frac{1}{\mathrm{J}}\,[\,\mathbf{F}\overline{\otimes}\mathbf{F}\,] : \mathbf{C} : [\,\mathbf{F}^{\mathrm{t}}\overline{\otimes}\mathbf{F}^{\mathrm{t}}\,]\,. \tag{24}$$

Last, we define the evolution of the growth multiplier ϑ according to [20], with

$$\dot{\vartheta} = \kappa(\vartheta)\phi(\boldsymbol{\Xi}) \tag{25}$$

where $\boldsymbol{\Xi}$ represents the growth stimulus. Here, $\kappa(\vartheta)$ is a limiting function that ensures that the tissue does not grow unboundedly [39],

$$\kappa(\vartheta) = \frac{1}{\tau}\left[\frac{\vartheta^{\max} - \vartheta}{\vartheta^{\max} - 1}\right]^{\gamma} \tag{26}$$

with $\partial_{\vartheta}\kappa(\vartheta) = -\gamma\kappa(\vartheta)/[\vartheta^{\max} - \vartheta]$, where $\vartheta^{\max}$ defines a growth threshold, and τ and γ control the speed and the non-linearity of the growth process [24]. The function $\phi(\boldsymbol{\Xi})$ represents the growth criterion similar to the flow rule in the theory of plasticity. In the following, we discuss two different approaches to drive the evolution of growth, stress driven and strain drive.

3.3 Numerical implementation

For the numerical implementation, we integrate the evolution of growth in time using an implicit Euler backward scheme,

$$\dot{\vartheta} = [\vartheta^{\mathrm{n}+1} - \vartheta^{\mathrm{n}}]/\Delta t\,, \tag{27}$$

where Δt denotes the current time increment. This allows us to introduce the discrete local residual

$$\mathcal{R} = \vartheta^{\mathrm{n}+1} - \vartheta^{\mathrm{n}} - \kappa(\vartheta)\phi(\boldsymbol{\Xi})\Delta t\,. \tag{28}$$

To solve this non-linear equation, we expand the residual up to the first order term. This allows us to solve the problem within a Newton iterative scheme according to the following equation,

$$\mathcal{R}(\vartheta)^{\mathrm{n}} + \partial_{\vartheta}\mathcal{R}(\vartheta)^{\mathrm{n}}\big|_{\vartheta^{\mathrm{n}}}[\vartheta^{\mathrm{n}+1} - \vartheta^{\mathrm{n}}] \doteq 0\,. \tag{29}$$

The tangent of the residual

$$\mathcal{K} = \mathrm{d}_{\vartheta}\mathcal{R} = 1 - [\kappa\partial_{\vartheta}\phi + \vartheta\partial_{\vartheta}\kappa]\,\Delta t \tag{30}$$

allows us to incrementally update the growth multiplier $\vartheta^{\mathrm{n}+1} \leftarrow \vartheta^{\mathrm{n}} - \mathcal{R}/\mathcal{K}$, determined by the current stimuli and loading history. Table 2 summarizes the local algorithmic treatment of the numerical procedure, which is embedded in the finite element framework on the constitutive level.

Table 2 Algorithm for implicit Euler scheme of strain-driven volumetric growth

Input: $\mathbf{F}^{t+1}, \vartheta^{t}$

1. Evaluate kinematics $\mathbf{C}^{t+1}, \mathbf{F}_{e}^{t+1} = \mathbf{F}^{t+1} \cdot \mathbf{F}_{g}^{t}$ and stresses $\mathbf{S}_{e}^{t+1}, \mathbf{S}^{t+1}$
2. Check for growth
   IF ($\lambda_{SMC} > \lambda_{crit}$)
   THEN Determine new growth multiplier
   WHILE $\mathcal{R} >$ tol DO
   Calculate residual $\mathcal{R} = \vartheta^{n+1} - \vartheta^{n} - \kappa(\vartheta)\phi(\boldsymbol{\Xi})\Delta t$
   Calculate tangent $\mathcal{K} = 1 - [\kappa\partial_{\vartheta}\phi + \vartheta\partial_{\vartheta}\kappa]\,\Delta t$
   Update growth $\vartheta^{n+1} \leftarrow \vartheta^{n} - \mathcal{R}/\mathcal{K}^{-1}$
   END
3. Compute Cauchy stresses $\boldsymbol{\sigma}^{t+1}$
   Compute tangent moduli $\mathbf{c}^{t+1}$

Output: $\boldsymbol{\sigma}^{t+1}, \mathbf{c}^{t+1}, \vartheta^{n+1}$

Remark 3 (Stress-driven anisotropic growth) *We first define the evolution of the growth multiplier ϑ in terms of a stress-based stimulus [20, 31],*

$$\dot{\vartheta} = \kappa(\vartheta)\phi(\mathbf{M}_{e})\,,$$

using a stress-driven growth criterion

$$\phi(\mathbf{M}_{e}) = \mathrm{tr}(\mathbf{M}_{e}) - \mathrm{M}_{crit}\,.$$

Here, $\mathbf{M}_{e} = \mathbf{C}_{e} \cdot \mathbf{S}_{e}$ is the elastic Mandel stress and M_{crit} denotes the physiological pressure above which growth occurs. The derivative of the growth criterion with respect to the growth multiplier ϑ required for the consistent linearization reads

$$\partial_{\vartheta}\phi = -\partial_{\vartheta}\mathbf{C}_{e} : \mathbf{S}_{e} + \mathbf{C}_{e} : \partial_{\vartheta}\mathbf{S}_{e}$$

with $\partial_{\vartheta}\mathbf{C}_{e} = -\mathbf{F}_{g}^{-t} \cdot \partial_{\vartheta}\mathbf{F}_{g}^{t} \cdot \mathbf{C}_{e} - \mathbf{C}_{e} \cdot \partial_{\vartheta}\mathbf{F}_{g} \cdot \mathbf{F}_{g}^{-1}$ and $\partial_{\vartheta}\mathbf{S}_{e} = \frac{1}{2}\,\mathbf{C}_{e} : \partial_{\vartheta}\mathbf{C}_{e}$. Finally, to complete the tangent moduli in (20), we provide the derivative of the growth multiplier with respect to the Cauchy-Green strain tensor, $\partial_{\mathbf{C}}\vartheta = \partial_{\mathbf{C}_{e}}\vartheta : \partial_{\mathbf{C}}\mathbf{C}_{e} = \kappa\Delta t[\,\frac{1}{2}\,\mathbf{C}_{e} : \mathbf{C}_{e} + \mathbf{S}_{e}\,]/\mathcal{K}$. Within a finite element setting, stress-driven growth requires an additional internal iteration to update the growth multiplier, since its driving force, the current stress, is typically not known a priori.

Remark 4 (Strain-driven anisotropic growth) *Alternatively, we could define the evolution of the growth multiplier ϑ in terms of a strain-based stimulus [20],*

$$\dot{\vartheta} = \kappa(\vartheta)\phi(\mathbf{F}_{e})\,,$$

using a strain-driven growth criterion

$$\phi(\mathbf{F}_{e}) = \lambda_{e} - \lambda_{crit} = \mathbf{F}_{e} : [\mathbf{n}_{z} \otimes \mathbf{n}_{z}] - \lambda_{crit}\,.$$

Here λ_{crit} denotes a physiological stretch above which growth occurs. We have assumed that the SMC are aligned with the collagen fibers in the extracellular matrix and that they undergo an affine deformation, meaning that their elastic stretches λ_{e} are approximately identical, $\lambda_{e} = \lambda_{SMC} = \lambda_{col} = \mathbf{F}_{e} : [\mathbf{n}_{z} \otimes \mathbf{n}_{z}]$. The remaining term for the tangent moduli then simply reads

$$\partial_{\vartheta}\phi = -\lambda/\lambda_{g}^{2}\,.$$

Unlike stress-driven growth, strain-driven growth does not require an additional internal iteration to update the growth multiplier, since its driving force, the current strain, is typically a priori known. Strain-driven growth is therefore computationally more stable and robust.

4 Arterial growth in hypertension

In this section we present some results of the two approaches described above and discuss their potential to model arterial growth due to hypertensive conditions.

4.1 Growth in a cylindrical prototype artery

In this first subsection, we explore a simple prototype model of growth in the arterial wall to illustrate the characteristic features of growth. We simulate an idealized artery slice, made up of media and adventitia layers. We choose the growth parameters to $\vartheta^{max} = 2$, $\gamma = 2$ and $\tau = 1$. We ask the question what driving force quantity is more suitable for hypertension-induced growth. To initiate growth, we adopt the following simulation protocol:

1. Gradually pressurize an artery up to the normotensive state at a physiological pressure of 13.3 kPa.
2. Calculate the resulting critical physiological stretches λ_{crit} and stresses M_{crit} locally and store their values in a pointwise fashion.
3. Apply the pressure up to the hypertensive state at a chronically elevated pressure of 16.0 kPa.
4. Allow the tissue to grow chronically to compensate for the extra deformation and stress.

Figures 4 and 5 illustrate a finite element simulation of growth in a cylindrical prototype artery. Figure 4 displays the maximum principal strains and stresses in a slice of the common carotid artery under normotensive and hypertensive conditions. Figure 5 compares the growth multiplier and the maximum principal stresses for strain- and stress-driven growth. The arterial wall thickness and the regional profiles of the growth multiplier differ substantially for the strain- and stress-driven cases.

For the stress-driven case, as displayed in Figure 5, bottom row, growth increases radially from inward to outward in a rather drastic way. Since the adventitia layer is much stiffer than the media layer, this results in higher stresses in the adventitia, making it grow much faster in the stress-driven case. Moreover, the higher growth rate

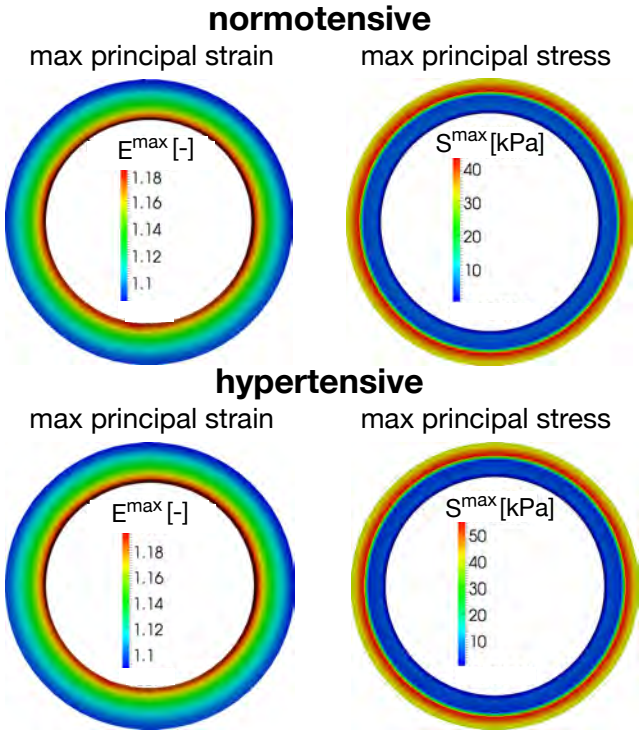

Fig. 4 Normotensive and hypotensive conditions in a cylindrical prototype artery with maximum principal strains, left, and stresses, right.

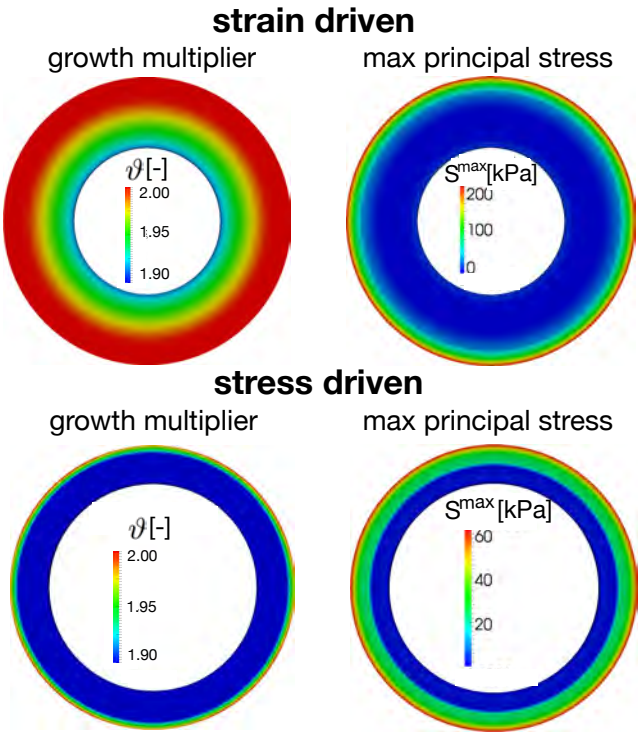

Fig. 5 Strain driven and stress driven growth in a cylindrical prototype artery with growth multiplier, left, and maximum principal stresses, right.

in the adventitia initiates a marked perpendicular expansion towards the center thereby decreasing the circumferential dimension of the media. For the strain-driven case, growth also increases radially, but significantly smoother than for the stress-driven case. For the first time, in contrast to previous studies [24, 52], we have simulated growth in an artery wall with distinct layers and distinct stiffnesses. Our results show that it is critical to account for the different properties in different layers to predict experimental findings. As we have discuss in the introduction, arterial thickening occurs meanly in the media, caused by hypertrophy and hyperplasia of SMC. For the stress-driven stimulus, growth seems to occur mainly in the adventitia layer which would contradict these findings.

Strain-driven growth, as displayed in Figure 5, top row, displays a more uniform growth distribution across the thickness. Since the circumferential stretch is more uniform than the stress distribution, growth occurs in a more distributed way, which seems to favorably agree with experimental findings.

The debate about the most adequate driving force for different processes in cells, e.g., cell differentiation or cell migration, remains vivid and still ongoing. Along these lines, the choice of a stress- or strain-driven approach to characterize hypertensive growth still remains unclear. From our results we conclude that growth in arterial tissue is highly sensitive to the choice of the underlying mechanical stimulus. In the particular case of growth in arteries it is known that growth occurs primarily in the media layer, since there is where the SMC are situated. To better characterize the constitutive response of the arterial wall, we will from now on assume that SMC growth is allowed to occur only in the media layer. Moreover, we will assume that stretch of the SMC is the mechanical variable that stimulates the growth process.

4.2 Growth in a human carotid artery

We now adopt the strain-driven approach towards arterial growth. According to Remark 4, the mechanical stimulus that triggers growth is the SMC stretch $\lambda_{\text{SMC}} = \lambda_{\text{e}} = \mathbf{F}_{\text{e}} : [\mathbf{n}_{\text{z}} \otimes \mathbf{n}_{\text{z}}]$, and the growth criterion is expressed as $\phi(\mathbf{F}_{\text{e}}) = \lambda_{\text{SMC}} - \lambda_{\text{crit}}$. To illustrate the features of the proposed approach, we compare our simulation with experimental findings [13]. We begin by studying the growth process in a slice of the common carotid artery as shown in Figure 6.

Figure 7, top, shows the evolution of a representative SMC in the medial layer of the common carotid artery. The SMC size increases in the radial direction while the longitudinal direction remains constant. Figure 7, bottom, shows the evolution of growth in a circular section of the common carotid artery at different time steps. In response to hypertension, the maximum growth mul-

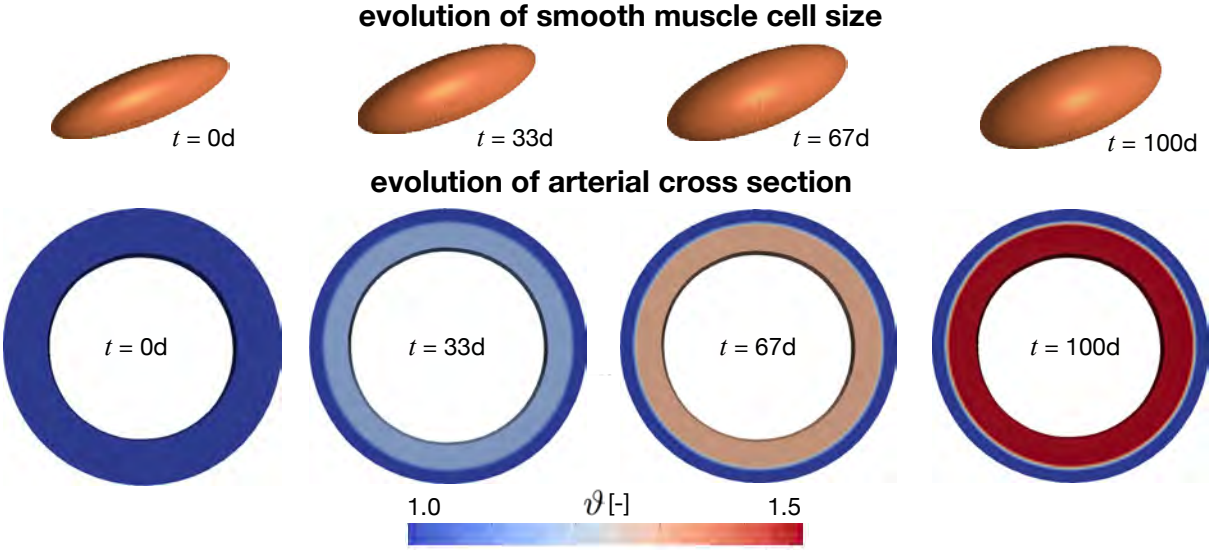

Fig. 7 Growth of a representative smooth muscle cell in the medial layer of the common carotid artery and its effect of the circular section at characteristic time steps. In response to hypertension, the growth multiplier gradually increases to $\vartheta = 1.47$, indicating an increase of smooth muscle cell thickness of almost 50%.

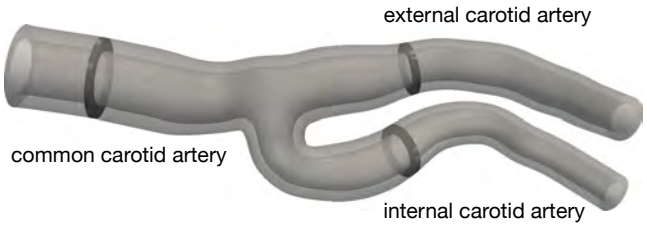

Fig. 6 Human carotid artery with three representative cross-sections in the common carotid artery, the internal carotid artery, and the external carotid artery, highlighted in dark.

tiplier increases to $\vartheta = 1.47$, indicating an increase of smooth muscle cell thickness of almost 50%.

Figure 8 shows the evolution of the growth multiplier over a period of 100 days, both for the experimental measurements in [13] and for the computational simulation with our model. Results displays a similar tendency throughout the growth process. Our results slightly overestimate the amount of growth during the first few days, and slightly underestimate the amount of growth long time.

Figure 9 displays the evolution of the maximum principal stresses in inner, media, and outer layers of a human carotid artery. Stresses in the media layer decrease as a result of SMC growth. SMC growth, myogenic tone, and other physiological process have the common goal to reduce elevated wall stress caused by hypertension. Their ultimate goal is to bring the wall stress back to its physiological range, i.e., reduce its values towards the normotensive situation. As the growth multiplier ϑ increases, the growth tensor $\mathbf{F}_{\mathrm{g}}$ increases and causes the elastic tensor $\mathbf{F}_{\mathrm{e}}$ to decrease. This reduces the elastic

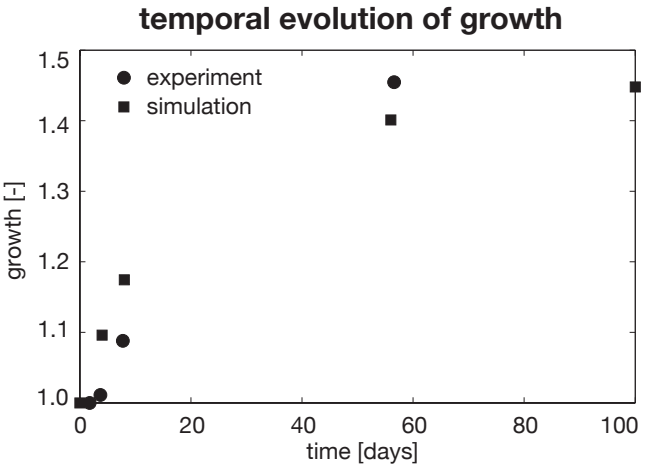

Fig. 8 Temporal evolution of growth in human carotid artery. Circles represent experimentally measured growth [13]; squares represent computationally simulated growth.

stress $\mathbf{S}_{\mathrm{e}}$. While the media layer grows and its stresses decrease, stresses in the adventitia layer undergo a substantial increase. The increase of adventitia stress is caused by the radial expansion of the media.

Figures 10 and 11 display growth in four representative longitudinal and transverse sections of the human carotid artery after $t = 100$ days of hypertension. Similar to the previous findings, growth is heterogeneous across the wall thickness, with smaller growth at the inner and larger growth at the outer layer. Growth also displays variations along the direction of flow.

Last, we summarize the spatio-temporal evolution of growth in three representative slices of the human carotid artery as highlighted in Figure 6. Figures 12, 13,

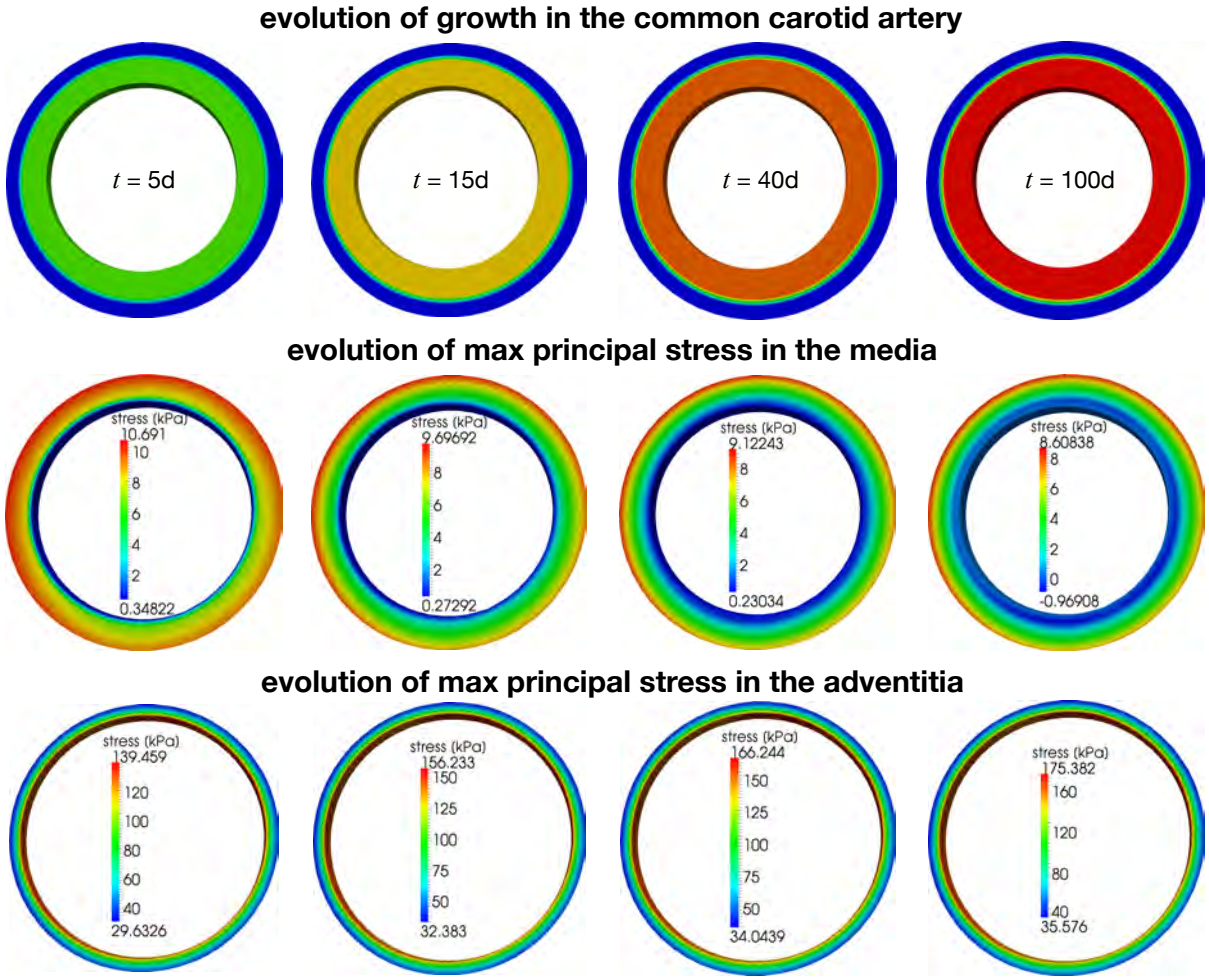

Fig. 12 Spatio-temporal evolution of growth in a representative slice of the common carotid artery. Growth multiplier, top, maximum principal stresses in the adventitia, middle, and maximum principal stresses in the media, bottom at 5, 15, 40, and 100 days of hypertension.

and 14 show the evolution of the growth multiplier, of the maximum principal stresses in the adventitia layer, and of the maximum principal stresses in the medial layer in the common, external, and internal carotid artery at four different time steps. Growth and stress display similar trends in all three sections. This is in agreement with the smooth variations in stretch between the normotensive and the hypertensive states. Stresses in the adventitia increase by 20%, while stresses in the media decrease by 25% in the common carotid artery, by 13% in the external carotid artery, and by 7% in the internal carotid artery, respectively.

5 Discussion

Growth and remodeling of living systems has advanced to a continuously growing field of research within the past decade [1]. Many recent studies focus on shedding light on different kinematic formulations, alternative balance equations, appropriate evolution equations, and suitable mechanical stimuli [43]. Here, we have adapted the classical kinematic decomposition of the deformation gradient into an elastic and a volumetric growth part [38, 51]. We have discussed microstructurally-motivated evolution equations for growth [21], and systematically compared different mechanical stimuli for the growth process [37]. To discretize the governing equations in time and space, we have applied an implicit Euler backward finite difference scheme in time and a geometrically nonlinear finite element scheme in space. To efficiently and robustly solve the set of governing equations, we have linearized the growth formulation consistently and embedded it locally at the integration point level.

We have shown that our model is capable of simulating hypertensive growth in arterial tissue. In particular, we have focused on growth-induced smooth muscle cell hypertrophy. We have assumed that when subject to mechanical stimuli, smooth muscle cells thicken in the radial direction, while their length remains virtually unchanged [21]. After comparing the two most common mechanical stimuli for growth, stress and strain, we have decided to choose the local smooth muscle cell stretch

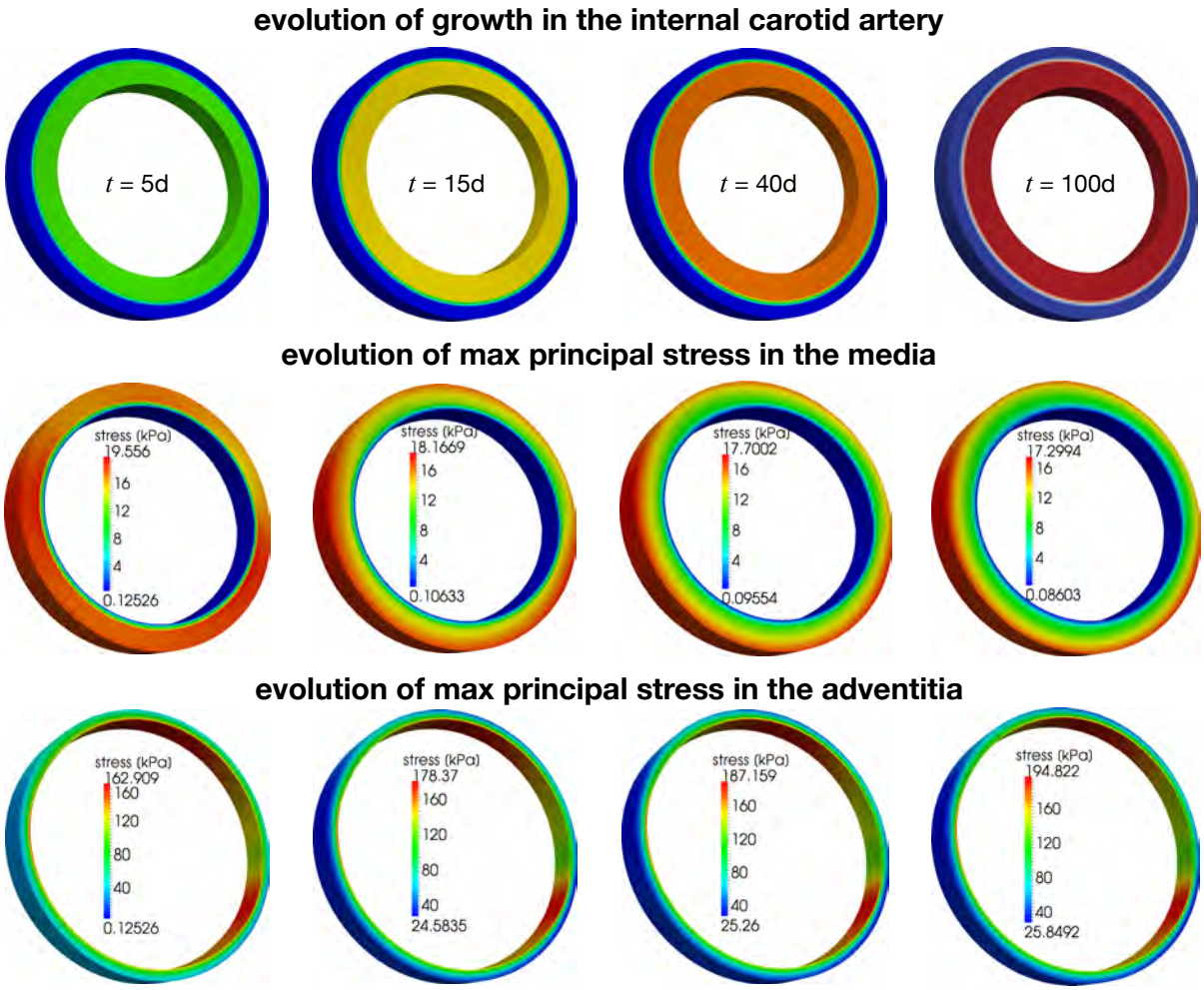

Fig. 13 Spatio-temporal evolution of growth in a representative slice of the internal carotid artery. Growth multiplier, top, maximum principal stresses in the adventitia, middle, and maximum principal stresses in the media, bottom at 5, 15, 40, and 100 days of hypertension.

as the stimulus for smooth muscle cell thickening. The resulting mathematical model allows us to explore how microstructural changes on the smooth muscle cell level translate into a macrostructural thickening of the arterial wall. This is conceptually similar to studying how microstructural changes of heart muscle cells translate into a macroscopic thickening of the ventricular wall in cardiac hypertension [50]. While microstructural changes in cardiac muscle cells [21] and skeletal muscle cells [64] have been attributed to sarcomerogenesis, the creation and deposition of new sarcomere units within the cell, microstructural changes in smooth muscle cells are far more complex and less well documented.

Our simulations display an excellent qualitative and quantitative agreement with experimental findings, both in terms of thickening and growth rates [13]. To demonstrate the potential of the proposed approach, we have shown the finite element simulation of a real patient-specific carotid geometry. Cerebral arteries are an object of intense investigation, since they are at high risk of uncontrolled growth, aneurysm formation [3, 60], and rupture [63]. Our results indicate a homogeneous growth throughout the medial layer along the entire carotid length. Only small portions of the carotid bifurcation displayed slightly elevated growth. While previous studies have mainly modeled the growing arterial wall as a single-layer system [24, 36], here, we have modeled the media and the adventitia as distinct layers with distinct mechanical properties [26]. This approach raises an interesting question related to the stress distribution. Stresses in the media layer decrease due to the radial growth of smooth muscle cells. This is a classical assumption in the adaptation of biological tissue. Smooth muscle cells respond, both acutely and chronically, to hypertension with the goal to bring the wall stress back to its physiological baseline state. Various interconnected mechanotransduction pathways in the cells are responsible for sensing the underlying mechanical stimuli [53,65]. In particular, smooth muscle cells are known to sense stretch in the extracellular matrix. Since smooth muscle cells are mainly present in the media and not in the adventitia, we have assumed that the media layer grows, while the

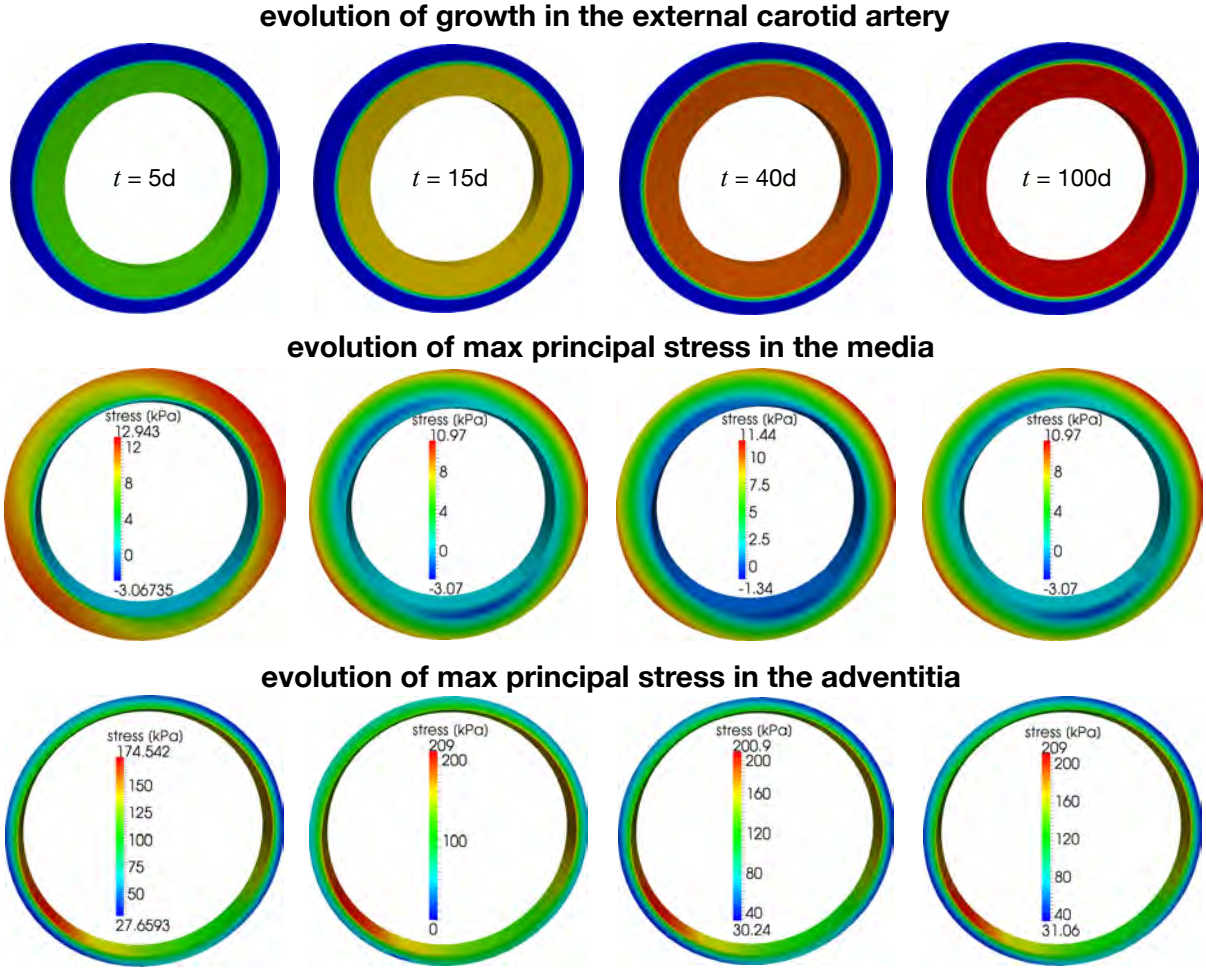

Fig. 14 Spatio-temporal evolution of growth in a representative slice of the external carotid artery. Growth multiplier, top, maximum principal stresses in the adventitia, middle, and maximum principal stresses in the media, bottom at 5, 15, 40, and 100 days of hypertension.

adventitia layer does not. Accordingly, the stresses in the adventitia increase up to a 20-30%, caused by combined effects of the elevated pressure and the growth of the media layer. These results reflect the well-accepted idea that the adventitia layer acts as a protection layer.

Despite these promising first results, we would like to address a few fundamental limitations of the current approach. First, our current model is based on purely passive baseline elasticity. Smooth muscle cells display an important active response, the myogenic tone, which allows the arterial wall to contract or expand acutely to maintain a baseline lumen [56]. Our arterial model would improve by the inclusion of this feature, although, up to date, only a few computational models of myogenic tone are available in literature [4, 9]. The underlying stimuli for growth could possibly include this basal tone. However, myogenic tone is a response to the overstretch of the smooth muscle cells, which we utilize as stimulus in our current model. We expect that the additional inclusion of basal tone could quantitatively scale our current growth response, but it would not qualitatively modify the growth response overall. Second, our current evolution equation for growth pre-imposes both the growth level and its rate. Its constitutive parameters could be calibrated experimentally to describe specific arteries and other cardiovascular tissues. At this point though, they lack of a real physiological interpretation. The challenge to tie the parameters to mechanotransduction pathways in arterial cells and tissue introduces an additional limitation. Experiments are usually performed in the normotensive state and in the final hypertensive state, but not in longitudinal studies to explore the transition between the two. Accordingly, most reported experiments do not allow us to calibrate our rate parameters. Moreover, experimental characterizations display huge variations across different species, across different arteries from the same species, and even across different specimen from the same artery.

In summary, we have adopted a well-established framework for volumetric growth to simulate hypertensive thickening of the human carotid artery. Our model makes a first attempt to link the key kinematic variable

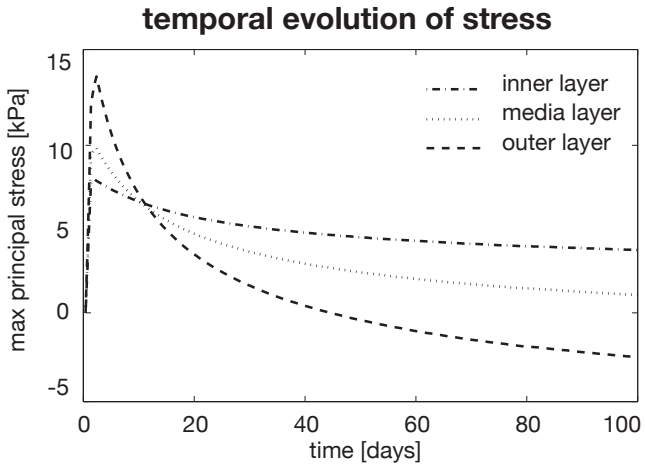

Fig. 9 Temporal evolution of maximum principal stresses in inner, media, and outer layers of human carotid artery.

of growth, a second order growth tensor, to microstructural changes of smooth muscle cells. The characterization of growth in terms of microstructural variables such as cell size and cell orientation smoothly integrates the multiscale nature of the living system into the mathematical model. Hypertensive arterial wall thickening is a critical medical condition since it may lead to decreases blood flow and other related complications. Computational models like ours can help to understand the underlying mechanochemical processes and provide a framework for biological and clinical researchers to jointly enhance the pharmagolocial or surgical management of hypertension.

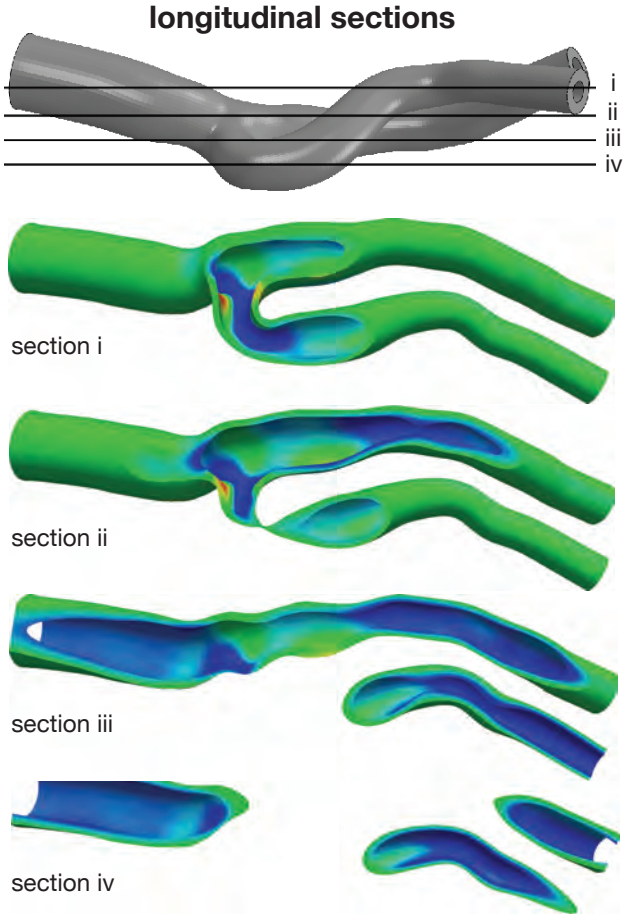

Fig. 10 Growth in different longitudinal sections of the human carotid artery at $t = 100$ days of hypertension.

References

1. Ambrosi D, Ateshian GA, Arruda EM, Cowin SC, Dumais J, Goriely A, Holzapfel GA, Humphrey JD, Kemkemer R, Kuhl E, Olberding JE, Taber LA, Garikipati K (2011) Perspectives on biological growth and remodeling. J Mech Phys Solids 59:863-883.
2. Ateshian GA (2007) On the theory of reactive mixtures for modeling biological growth. Biomech Model Mechanbio 6:423-445.
3. Bazilevs Y, Hsu MC, Zhang Y, Wang W, Liang X, Kvamsdal T, Brekken R, Isaken JG (2010) A fully-coupled fluid-structure interaction simulation of cerebral aneurysms. Comp Mech, 46:3-16.
4. Böl M, Schmitz A, Nowak G, Siebert T (2012) A three-dimensional chemo-mechanical continuum model for smooth muscle contraction. J Mech Behav Biomed Mater 13:215-229.
5. Boutouyrie P, Bussy C, Lacolley P, Girerd X, Laloux B, Laurent S (1999) Association between local pulse pressure, mean blood pressure, and large-artery remodeling. Circulation 100:1387-1393.
6. Brayden JE, Nelson MT (1992) Regulation of arterial tone by activation of calcium-dependent potassium channels. Science 256:532-535.
7. Davis MJ, Hill MA (1999) Signaling mechanisms underlying the vascular myogenic response. Physiol Rev 79:387-423.
8. Eberth JF, Popovic N, Gresham VC, Wilson E, Humphrey JD (2010) Time course of carotid artery growth and remodeling in response to altered pulsatility. Am J Phys Heart Circ Phys 299:H1875-H1883.
9. Famaey N, vanSloten J, Kuhl E (2013) A three-constituent damage model for arterial clamping in computer-assisted surgery. Biomech Model Mechanbio 12:123-136.
10. Feihl F, Liaudet L, Levy BI, Waeber B (2008) Hypertension and microvascular remodelling. Cardiovas Res 78:274-285.
11. Flory PJ (1961) Thermodynamic relations for high elastic materials. T Faraday Soc 57:829-838.
12. Folkow B, Grimby G, Thulesius O (1958) Adaptive structural changes of the vascular walls in hypertension and their relation to the control of the peripheral resistance. Acta Physiol Scand 44:255-272.
13. Fridez P, Makino A, Kakoi D, Miyazaki H, Meister JJ, Hayashi K, Stergiopulos N (2002) Adaptation of conduit artery vascular smooth muscle tone to induced hypertension. Ann Biomed Eng 30:905-916.
14. Fung YC, Liu S (1989) Change of residual strains in arteries due to hypertrophy caused by aortic constriction.

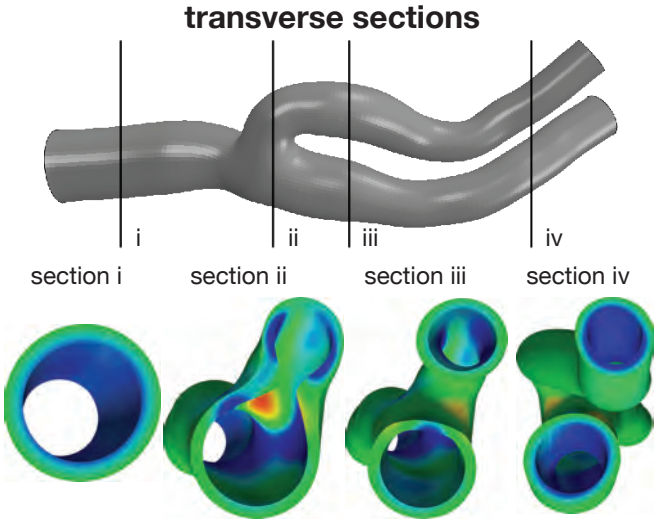

Fig. 11 Growth in different transverse sections of the human carotid artery at $t = 100$ days of hypertension.

Circ Res 65:1340-1349.
15. Ganghoffer JF (2010) Mechanical modeling of growth considering domain variation. Part II: Volumetric and surface growth involving Eshelby tensors. J Mech Phys Solids 58:1434-1459.
16. Gasser TC, Holzapfel GA (2002) A rate-independent elastoplastic constitutive model for biological fiber-reinforced composites at finite strains. Comp Mech, 29:340-360.
17. Garcia A (2012) Experimental and numerical framework for modelling vascular diseases and medical devices. PhD thesis, University of Zaragoza, Spain.
18. Gleason RL, Humphrey JD (2004) A mixture model of arterial growth and remodeling in hypertension: Altered muscle tone and tissue turnover. J Vasc Res 41:352-363.
19. Gleason RL, Humphrey JD (2005) Effects of a sustained extension on arterial growth and remodeling: a theoretical study. J Biomech 38:1255-1261.
20. Göktepe S, Abilez OJ, Kuhl E (2010) A generic approach towards finite growth with examples of athlete's heart, cardiac dilation, and cardiac wall thickening. J Mech Phys Solids 58:1661-1680.
21. Göktepe S, Abilez OJ, Parker KK, Kuhl E (2010) A multiscale model for eccentric and concentric cardiac growth through sarcomerogenesis. J Theor Biol 265:433-442.
22. Goriely A, BenAmar M (2007) On the definition and modeling of incremental, cumulative, and continuous growth laws in morphoelasticity. Biomech Model Mechanobio, 6:289-296.
23. Haga JH, Li YSJ, Chien S (2007) Molecular basis of the effects of mechanical stretch on vascular smooth muscle cells. J Biomech 40:947-960.
24. Himpel G, Kuhl E, Menzel A, Steinmann P (2005) Computational modelling of isotropic multiplicative growth. CMES Comp Model Eng Sci 8:119-134.
25. Holzapfel GA (2000) Nonlinear Solid Mechanics: A Continuum Approach for Engineering. John Wiley & Sons.
26. Holzapfel GA, Gasser TC, Ogden RW (2000) A new constitutive framework for arterial wall mechanics and a comparative study of material models. J Elasticity, 61:1-48.
27. Humphrey JD, Rajagopal KR (2003) A constrained mixture model for arterial adaptations to a sustained step change in blood flow. Biomech Model Mechanbio, 2:109-126.
28. Humphrey JD (2009) Need for a continuum biochemomechanical theory of soft tissue and cellular growth and remodeling. in Biomechanical Modelling at the Molecular, Cellular and Tissue Levels. Springer Vienna.
29. Humphrey JD, Rajagopal KR (2002) A constrained mixture model for growth and remodeling of soft tissues. Math Models Methods Appl Sci 12:407-430.
30. Imatani S, Maugin GA (2002) A constitutive model for material growth and its application to three-dimensional finite element analysis. Mech Res Comm 29:477-483.
31. Klepach D, Lee LC, Wenk JF, Ratcliffe MB, Zohdi TI, Navia JA, Kassab GS, Kuhl E, Guccione JM (2012) Growth and remodeling of the left ventricle. Mech Res Comm 42,134-141.
32. Klisch SM, Sah RL, Hoger A (2005) A cartilage growth mixture model for infinitesimal strains: solutions of boundary-value problems related to in vitro growth experiments. Biomech Model Mechanbio 3:209-223.
33. Kuhl E, Menzel A, Steinmann P (2003) Computational modeling of growth. Comp Mech 32:71-88.
34. Kuhl E, Steinmann P (2003) Theory and numerics of geometrically non-linear open system mechanics. Int J Numer Meth Eng 58:1593-1615.
35. Kuhl E, Steinmann P (2003) Mass- and volume specific views on thermodynamics for open systems. Proc Roy Soc London 459:2547-2568.
36. Kuhl E, Maas R, Himpel G, Menzel A (2007) Computational modeling of arterial wall growth. Biomech Model Mechanbio 6:321-331.
37. Kuhl E, Holzapfel GA (2007) A continuum model for remodeling in living structures. J Mater Sci 42:8811-8823.
38. Lee EH (1969) Elastic-plastic deformation at finite strains. J Appl Mech 36:1-6.
39. Lubarda VA, Hoger A (2002) On the mechanics of solids with a growing mass. Int J Solids & Structures 39:4627-4664.
40. Marsden JE, Hughes TJR (1994) Mathematical Foundations of Elasticity. Dover Publications.
41. Menzel A. Modelling of anisotropic growth in biological tissues. Biomech Model Mechanobio 3:147-171.
42. A. Menzel. A fibre reorientation model for orthotropic multiplicative growth. Biomech Model Mechanobio 6:303-320.
43. Menzel A, Kuhl E (2012) Frontiers in growth and remodeling. Mech Res Comm 42:1-14.
44. Mulvany MJ, Aalkjaer C (1990) Structure and function of small arteries. Physiol Rev 70:921-961.
45. O'Connell MK, Murthy S, Phan S, Xu C, Buchanan J, Spilker R, Dalman RL, Zarins CK, Denk W, Taylor CA (2008) The three-dimensional micro- and nanostructure of the aortic medial lamellar unit measured using 3d confocal and electron microscopy imaging. Matrix Biology 27:171-181.
46. Osol G (1995) Mechanotransduction by vascular smooth muscle. J Vasc Res 32:275-292.

47. Owens GK. Control of hypertrophic versus hyperplastic growth of vascular smooth-muscle cells. Am J Physiol 257:H1755-H1765.
48. Owens GK, Schwartz SM (1983) Vascular smooth-muscle cell hypertrophy and hyperploidy in the goldblatt hypertensive rat. Circ Res 53:491-501.
49. Owens GK, Rabinovitch PS, Schwartz SM (1981) Smooth-muscle cell hypertrophy versus hyperplasia in hypertension. Proc Nat Acad Sci 78:7759-7763.
50. Rausch M, Dam A, Göktepe S, Abilez OJ, Kuhl E (2011) Computational modeling of growth: Systemic and pulmonary hypertension in the heart. Biomech Model Mechanobio 10:799-811.
51. Rodriguez EK, Hoger A, McCulloch AD (1994) Stress-dependent finite growth in soft elastic tissues. J Biomech 27:455-467.
52. Rodriguez J, Goicolea JM, Gabaldon F (2007) A volumetric model for growth of arterial walls with arbitrary geometry and loads. J Biomech 40:961-971.
53. Saez P, Pena E, Martinez M, Kuhl E (2013) Mathematical modeling of collagen turnover in biological tissue. J Math Bio doi:10.1007/s00285-012-0613-y.
54. Saez P, Pena E, Martinez M (2013) On the microstructural modeling of patient-specific human carotid artery. submitted for publication.
55. Schofield I, Malik R, Izzard A, Austin C, Heagerty A (2002) Vascular structural and functional changes in type 2 diabetes mellitus - evidence for the roles of abnormal myogenic responsiveness and dyslipidemia. Circulation 106:3037-3043.
56. Schubert R, Mulvany MJ (1999) The myogenic response: established facts and attractive hypotheses. Clinical Science 96:313-326.
57. Skalak R, Dasgupta G, Moss M, Otten E, Dullemeijer P, Vilmann H (1982) Analytical description of growth. J Theor Biol 94:555-577.
58. Sommer G, Holzapfel GA. 3d constitutive modeling of the biaxial mechanical response of intact and layer-dissected human carotid arteries. J Mech Behav Biomed 5:116-128.
59. Taber LA (1995) Biomechanics of growth, remodeling, and morphogenesis. Appl Mech Rev 48:487-545.
60. Takizawa K, Schjodt K, Puntel A, Kostov N, Texduyar TE (2012) Patient-specific computer modeling of blood flow in cerebral arteries with aneurysm and stent. Comp Mech, 50:675-686.
61. Thakar RG, Cheng Q, Patel S, Chu J, Nasir M, Liepmann D, Komvopoulos K, Li S. Cell-shape regulation of smooth muscle cell proliferation. Biophys J 96:3423-3432.
62. Wiener J, Loud AV, Giacomelli F, Anversa P (1977) Morphometric analysis of hypertension-induced hypertrophy of rat thoracic aorta. Am J Pathol 88:619-633.
63. Zohdi TI, Holzapfel GA, Berger SA (2004) A phenomenological model for atherosclerotic plaque growth and rupture. J Theor Bio 227:437-443.
64. Zöllner AM, Abilez OJ, Böl M, Kuhl E (2012) Stretching skeletal muscle - chronic muscle lengthening through sarcomerogenesis. PLoS ONE 7:e45661.
65. Zöllner AM, Buganza-Tepole A, Kuhl E (2012) On the biomechanics and mechanobiology of growing skin. J Theor Bio 297:166-175.